Title

Branched-chain keto acids inhibit mitochondrial pyruvate carrier and suppress gluconeogenesis in hepatocytes.

Journal

Cell Reports, 42(6)

Authors

Nishi, Kiyoto
Yoshii, Akira
Abell, Lauren
et al.

Publication Date

2023-06-27

DOI

10.1016/j.celrep.2023.112641

Peer reviewed

HHS Public Access

Author manuscript

Cell Rep. Author manuscript; available in PMC 2023 October 23.

Published in final edited form as:

Cell Rep. 2023 June 27; 42(6): 112641. doi:10.1016/j.celrep.2023.112641.

Branched-chain keto acids inhibit mitochondrial pyruvate carrier and suppress gluconeogenesis in hepatocytes

Kiyoto Nishi[1,3], **Akira Yoshii**[1], **Lauren Abell**[1], **Bo Zhou**[1], **Ricardo Frausto**[4], **Julia Ritterhoff**[1], **Timothy S. McMillen**[1], **Ian Sweet**[2], **Yibin Wang**[4,5], **Chen Gao**[4,6,*], **Rong Tian**[1,7,*]

[1]Mitochondria and Metabolism Center, Department of Anesthesiology and Pain Medicine, University of Washington, 850 Republican Street, Seattle, WA 98109, USA

[2]University of Washington Medicine Diabetes Institute, University of Washington, 750 Republican Street, Seattle, WA 98109, USA

[3]Department of Pharmacology, Shiga University of Medical Science, Otsu, Shiga 520-2182, Japan

[4]Department of Anesthesiology, Cardiovascular Research Laboratories, David Geffen School of Medicine, University of California Los Angeles, Los Angeles, CA 90095, USA

[5]Signature Program in Cardiovascular and Metabolic Diseases, Duke-NUS School of Medicine, Singapore, Singapore

[6]Department of Pharmacology and Systems Physiology, University of Cincinnati, College of Medicine, Cincinnati, OH 45267-0575, USA

[7]Lead contact

SUMMARY

Branched-chain amino acid (BCAA) metabolism is linked to glucose homeostasis, but the underlying signaling mechanisms are unclear. We find that gluconeogenesis is reduced in mice deficient of *Ppm1k*, a positive regulator of BCAA catabolism, which protects against obesity-induced glucose intolerance. Accumulation of branched-chain keto acids (BCKAs) inhibits glucose production in hepatocytes. BCKAs suppress liver mitochondrial pyruvate carrier (MPC) activity and pyruvate-supported respiration. Pyruvate-supported gluconeogenesis is selectively suppressed in *Ppm1k*-deficient mice and can be restored with pharmacological activation of BCKA catabolism by BT2. Finally, hepatocytes lack branched-chain aminotransferase that alleviates BCKA accumulation via reversible conversion between BCAAs and BCKAs. This

*Correspondence: gaoc3@ucmail.uc.edu (C.G.), rongtian@uw.edu (R.T.).

AUTHOR CONTRIBUTIONS

K.N. and R.T. designed the study and wrote the manuscript. K.N., A.Y., L.A., B.Z., J.R., and T.S.M. performed most experiments. I.S. advised on ^{14}C-pyruvate uptake assay and subsequent data analyses. Y.W. generated the *Ppm1k*-deficient mice. R.F., C.G., and Y.W. carried out liver-specific *Bckdha*-deficient mice study. R.T. oversaw the project.

DECLARATION OF INTERESTS

The authors declare no competing interests.

SUPPLEMENTAL INFORMATION

Supplemental information can be found online at https://doi.org/10.1016/j.celrep.2023.112641.

renders liver MPC most susceptible to circulating BCKA levels hence a sensor of BCAA catabolism.

In brief

Nishi et al. report that mice with impaired BCAA catabolism due to *Ppm1k* deficiency show reduced gluconeogenesis. Mechanistically, accumulated BCKAs inhibit liver MPC activity, resulting in reduced glucose production from pyruvate. Furthermore, BCATm in non-hepatic mitochondria mitigates the inhibition of MPC by converting BCKAs into BCAAs.

Graphical Abstract

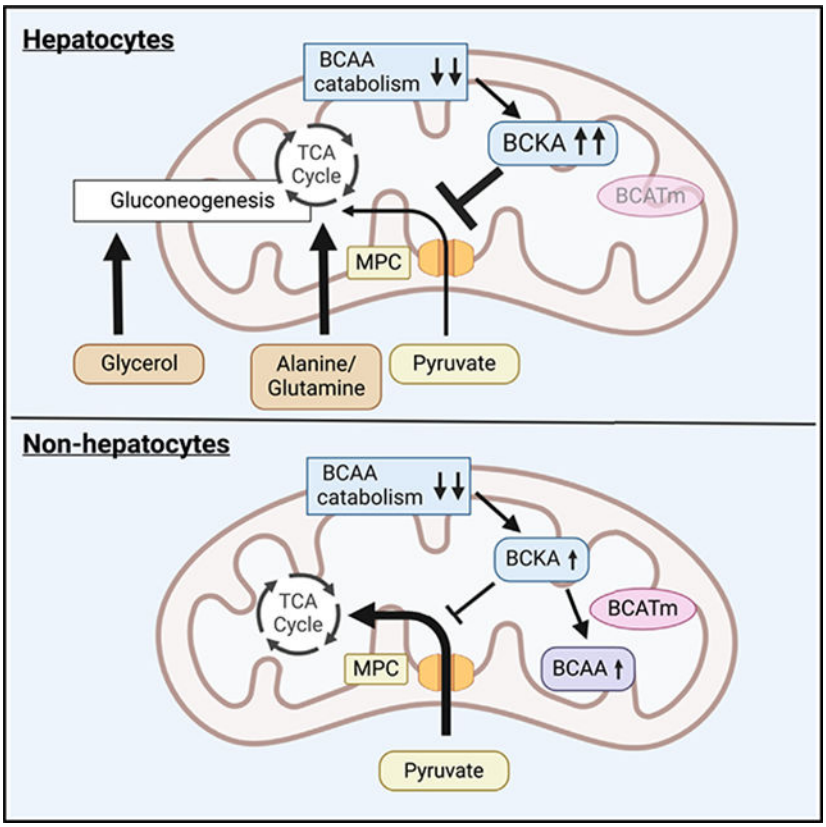

INTRODUCTION

Branched-chain amino acids (BCAAs), i.e., leucine, isoleucine, and valine, are essential amino acids in mammals; BCAA level *in vivo* is highly dependent on their catabolism in mitochondria.[1] The rate-limiting step of BCAA catabolism is catalyzed by the branched-chain ketoacid dehydrogenase (BCKDH) complex, which is regulated through dephosphrylation (activation)/phosphorylation (inactivation) mechanisms.[2–4] A mitochondria-localized phosphatase (also known as PP2Cm), encoded by *Ppm1k*, acts as the primary activator of BCKDH in mice.[5]

Recent studies have linked BCAA metabolism to glucose homeostasis. Circulating levels of BCAAs and related metabolites are positively correlated with obesity and glucose intolerance,[6–11] and they predict the risk of future type 2 diabetes.[12–14] Furthermore, impaired BCAA catabolism disrupts glucose utilization and causes mitochondrial dysfunction.[15–18] Restricting BCAA intake or increasing their catabolism by activating the BCKDH complex improves glucose tolerance in obesity rodent models.[9,11,19,20] These observations suggest that accumulation of metabolites upstream of BCKDH complex, i.e., BCAAs or BCKAs impair glucose homeostasis. However, the molecular mediators via which BCAAs or BCKAs modulate glucose homeostasis remain elusive. Furthermore, whole-body deletion (knockout [KO]) of *Ppm1k*, which inhibits BCKDH and increases circulating BCAA and BCKA levels, does not cause glucose intolerance or insulin resistance.[15–18]

Unlike other amino acids, systemic BCAA catabolism involves communication between the liver and peripheral organs. Due to the lack of branched-chain aminotransferase (BCAT), the liver does not participate in the first step of BCAA catabolism, i.e., the conversion of BCAAs to BCKAs. Instead, BCKAs released from other organs, e.g., skeletal muscle, are oxidized in the liver.[21,22] Recent studies suggest that decreased activity of the liver BCKDH complex in obesity shifts BCKA oxidation from liver to skeletal muscle, which disturbs lipid metabolism in muscle, causing insulin resistance.[9,23] Using *Ppm1*k KO mice, here we ask whether and how reduced BCKA oxidation affects liver metabolism. We find that failure of oxidation and subsequent accumulation of BCKAs in the liver inhibits mitochondrial pyruvate carrier activity, resulting in suppression of gluconeogenesis from pyruvate. These results reveal an important role of the liver in coordinating glucose and BCAA metabolism by acting as a sensor of circulating BCKA level.

RESULTS

Gluconeogenesis is suppressed in Ppm1k-deficient mice

Whole-body deletion (KO) of *Ppm1k*, which encodes a mitochondria-localized protein phosphatase (also known as PP2Cm), results in inactivation of BCKDH and elevated serum levels of BCAAs and BCKAs in mice (Table S1).[15–17] The *Ppm1k* KO mice, both males and females, showed normal body weight (Figures S1A and S1D) and unaltered glucose tolerance (Figures S1B and S1E) compared with wild-type (WT) control mice. No differences were observed between WT and KO in the insulin tolerance test (Figures S1C and S1F) or blood glucose levels in the fed or overnight fasted state (Figures S1G and S1H). These observations are consistent with prior reports that the KO mice, despite high circulating levels of BCAAs and BCKAs, do not develop insulin resistance.[15,17] Interestingly, the KO mice showed slightly but significantly elevated serum lactate (Figure 1A) and β-hydroxybutyrate (Figure 1B) levels after overnight fasting. Moreover, the respiratory exchange range (RER) in the KO mice trended lower during the non-feeding phase (Figure S1I). These findings suggest increased fatty oxidation and ketogenesis in the KO mice. To determine whether KO mice had deficiency in gluconeogenesis, we performed the pyruvate tolerance test in overnight fasted mice and found significantly lower blood glucose levels after pyruvate challenge in KOs of both sexes (Figures 1C and 1D).

Elevated gluconeogenesis is known to contribute to hyperglycemia and glucose intolerance in obesity and type II diabetes.[24–26] We thus investigated whether deletion of *Ppm1k* could reduce gluconeogenesis, lower fasting glucose levels, and improve glucose intolerance in obese mice. KO mice fed with 60% high-fat diet (HFD; Research Diets, D12492) from 9 weeks old for 18 weeks showed the same weight gain as HFD-fed WT (Figure S1J). However, glucose production after pyruvate challenge was significantly suppressed (Figure 1E) and glucose tolerance was improved (Figure 1F) in KO compared with WT after 4 weeks of HFD feeding, and the trend was maintained at 18 weeks (Figures 1G and 1H). Furthermore, fasting blood glucose was lower in KO mice after 18 weeks of HFD feeding (Figure 1I), while insulin resistance did not differ between HFD-fed WT and KO (Figures S1K and S1L). Together, these results suggest that *Ppm1k* deletion suppresses glucose production from pyruvate and improves glucose tolerance in mice with diet-induced obesity.

High level of BCKAs suppresses glucose production in isolated hepatocyte

To determine whether the reduction of pyruvate-supported glucose production is hepatocyte autonomous, we performed *in vitro* glucose production assay[27] using hepatocytes isolated from WT and KO mice. WT and KO hepatocytes showed the same glucose production when BCAA/BCKA free buffer was used (Figure 2A). The mRNA and protein expression levels of key enzymes involved in gluconeogenesis,[25] glucose-6-phosphatase (G6Pase), phosphoenolpyruvate carboxykinase (Pck1), fructose-1,6-bisphosphatase 1 (FBP1), and pyruvate carboxylase (PCx) did not differ between WT and KO (Figures 2B, 2C, S2A, and S2B). These results suggested that the gluconeogenesis machinery in KO was intact. Liver BCAA levels were unchanged in KO (Figure 2D) despite elevated serum BCAA levels (Table S1). Furthermore, adding BCAAs to the assay buffer resulted in a modest and identical reduction of glucose production in both WT and KO hepatocytes (Figure S2C). These results suggest that elevated BCAAs are unlikely the culprit of reduced gluconeogenesis in KO mice.

BCKA levels were markedly elevated in KO liver (Figure 2D).[17,28] Loading primary hepatocytes with BCKAs in culture resulted in significantly higher intracellular BCKA levels in KO hepatocytes in a dose-dependent manner (Figure 2E). Furthermore, addition of BCKAs to WT hepatocyte culture moderately increased glucose production in the absence of other substrates, and the effect became minimal in the presence of pyruvate/lactate, suggesting that BCKA oxidation was a minor contributor to gluconeogenesis (Figures 2F and 2G). In KO hepatocytes, BCKAs had little effect on glucose production without other substrates, consistent with their inability to oxidize BCKAs. Moreover, BCKAs significantly reduced glucose production from pyruvate/lactate in KO (Figures 2F and 2G). These results suggest that accumulation of BCKAs due to defective catabolism suppresses glucose production from pyruvate/lactate. To rule out the possibility that *Ppm1k* deletion affected other proteins than BCKDH, we tested the effect of BCKAs on glucose production in hepatocytes isolated from mice with liver-specific deletion of *Bckdha* (BCKDHa-LKO) and observed similar suppression (Figures S2D–S2F). The BCKDHa-LKO mice on HFD also showed better glucose tolerance, while chow-fed BCKDHa-LKO had similar glucose tolerance to control mice (Figures 2H and S2G). In addition, we stimulated BCKDH activity in KO with 3,6-dichlorobrenzo(b)thiophene-2carboxylic acid (BT2), a small-molecule

inhibitor of BDK,[15,20] and BT2 treatment elevated glucose levels after pyruvate challenge in KO but showed no significant effect in WT mice (Figures 2I and S2H). Together, these results indicate that catabolism of BCKAs is a critical mechanism regulating the utilization of pyruvate/lactate for gluconeogenesis in hepatocytes.

BCKAs selectively suppresses pyruvate-supported glucose production

In addition to pyruvate, the substrates for gluconeogenesis include glutamine, alanine, and glycerol. Each substrate enters the final common pathway of gluconeogenic via distinct routes to produce glucose (Figure 2B). For examples, hepatocytes deficient in glutaminase 2 (essential enzyme for the conversion of glutamine to glutamate) show significantly impaired glutamine-driven glucose production, while pyruvate-/lactate-driven glucose production is maintained.[29] To determine which step of glucose production is affected by BCKAs, we measured pyruvate-, alanine-, glycerol-, and glutamine-supported glucose production in BCKA-treated and control hepatocytes. To our surprise, only pyruvate-supported glucose production was suppressed by BCKAs (Figure 2J). Consistent with the *in vitro* results, blood glucose levels after alanine or glycerol challenge did not differ between KO and WT in both male and female mice (Figures 2K, 2L, S2I, and S2J). Collectively, these results suggest that accumulation of BCKAs in hepatocytes of KO mice specifically suppresses pyruvate-supported glucose production.

BCKAs regulate pyruvate-supported glucose production through inhibiting mitochondrial pyruvate carrier

To further explore the role of BCKAs in liver mitochondrial function, we measured the respiration of liver mitochondria treated with BCKAs using a variety of complex I substrates. While pyruvate-/malate-supported respiration was suppressed by BCKAs (Figures 3A and 3B), glutamate-/malate-supported respiration was unaltered (Figures 3C and 3D), indicating that not complex I activity but pyruvate utilization upstream of complex I is suppressed by BCKAs. UK5099, an inhibitor of mitochondrial pyruvate carrier (MPC), reduced respiration of WT and KO to the same level regardless of the presence of BCKA when pyruvate/malate were used as substrates (Figures 3A and 3B). Note that UK5099 did not affect glutamate-/malate-supported respiration in any groups (Figures 3C and 3D). BCKAs were previously shown not alter pyruvate dehydrogenase (PDH) activity[15]; thus, we interpreted these results as BCKAs inhibiting MPC activity. In a glucose production assay using pyruvate/lactate as substrates, which requires MPC but is independent of PDH activity, metabolite profiling by gas chromatography-mass spectrometry (GC-MS) showed that pyruvate and lactate levels increased while intermediates in gluconeogenesis decreased in hepatocytes treated with BCKAs (Figure 3E). In these hepatocytes, levels of glutamate and alanine, which could enter mitochondria via MPC-independent mechanisms,[30,31] decreased. Treatment with UK-5099, that pharmacologically inhibited MPC in hepatocytes, phenocopied the metabolite profile (Figure 3E). When we tracked pyruvate/lactate fate using ^{13}C-pyruvate in the glucose production assay, we found that BCKAs altered M+3 enrichment of TCA cycle metabolites in the same direction as UK-5099 (Figure 3F). Moreover, we found that UK5099 canceled BCKAs' effects on glucose production (Figure 3G). Finally, we overexpressed Mpc1 and 2 in HepG2 cells (Figure 3H), a human hepatocyte cell line in which BCKAs suppress glucose production (Figure S3A). As shown in Figures

3I and S3B, the suppression of glucose production by BCKAs was significantly blunted in MPC1/2-overexpressing (OE) hepatocytes, confirming that the suppression of glucose production by BCKAs was mediated by MPC inhibition. Together, these data indicate that BCKAs regulate liver mitochondrial pyruvate utilization and glucose production through controlling MPC activity.

Mammalian MPC is a heterooligomeric complex that consists of two essential components, Mpc1 and Mpc2.[32] Two recent studies independently reported that hepatocyte-specific deletion of Mpc1[30] or Mpc2[31] suppressed pyruvate-supported gluconeogenesis and improved glucose tolerance in obese mice. While these studies provided supporting evidence that reduced gluconeogenesis in KO could be attributable to the inhibition of MPC, regulatory mechanisms of MPC activity are virtually unknown.

The expression levels of MPC1 and MPC2 in liver tissue (Figures 3J and 3K) or isolated liver mitochondria (Figures S3C and S3D) did not differ between WT and KO. Therefore, we hypothesized that BCKAs regulated MPC function. To determine whether BCKAs directly inhibit MPC activity, we measured ^{14}C-labeled pyruvate uptake in isolated mitochondria.[33] While pyruvate uptake did not differ between WT and KO in the absence of BCKAs (Figure 3L), BCKAs dose-dependently inhibited pyruvate uptake in both WT and KO liver mitochondria (Figure 3M). MPC inhibition by BCKAs was significantly greater in KO compared with WT mitochondria at 10 and 33.3 μM BCKAs (Figure 3M). This is likely due to the inability of KO mitochondria to catabolize BCKAs, resulting in a greater accumulation of BCKAs (Figure S3E). Although BCKAs and pyruvate bear structural similarity, the inhibition of MPC by BCKAs was unlikely due to competitive binding of substrate. Half maximal inhibitory concentration (IC_{50}) values for BCKAs did not change when pyruvate concentration increased from 15 to 150 μM in the mitochondrial pyruvate uptake assay (Figures 3N and 3O), suggesting that BCKAs inhibited MPC activity in a non-competitive manner.[34] Next, we determined whether BCKAs directly interact with MPC by DARTs (drug affinity responsive target stability) assay,[35,36] which utilizes the principle that proteins become less susceptible to proteases when binding with small molecules/metabolites.[37] We assessed the protease susceptibility of MPC1, MPC2, and GAPDH in the presence/absence of BCKAs and found that protease susceptibility of MPC1 was reduced by BCKAs (Figures 3P and 3Q). Importantly, BCKAs did not change the susceptibility of GAPDH (Figures S3F and S3G), indicating that protease activity itself was not altered by BCKAs. This observation suggests that a direct interaction of BCKAs with MPC1 leads to the inhibition. High BCKAs could cause covalent modification of the MPC, hence altering its activity. This is unlikely, though, given that KO and WT mitochondria demonstrated similar pyruvate uptake when BCKAs were absent in the assay buffer.

Mitochondrial BCAA aminotransferase (BCATm) reaction attenuates the inhibitory effect of BCKAs in non-liver mitochondria

To determine whether BCKAs inhibit MPC in non-liver mitochondria, we assessed MPC function in cardiac mitochondria. Neither MPC1/2 expression levels (Figure S4A) nor pyruvate uptake without BCKAs differ in cardiac mitochondria from WT and KO mice (Figure 4A). Unlike liver, 33.3 μM BCKAs inhibited pyruvate uptake to the same

extent in WT and KO heart mitochondria (Figure S4B). Furthermore, the suppression of pyruvate uptake by BCKAs in KO cardiac mitochondria was markedly less than KO liver mitochondria (Figure 4B), suggesting a differential in the sensitivity to BCKAs. We and others have shown that pyruvate-/malate-supported respiration was decreased in cardiac mitochondria of KO mice and attributed the change to reduced O-linked GlcNacylation of PDH.[15,16] Although BCKAs were found not to inhibit PDH activity, whether they contributed to reduced respiration by inhibiting MPC has not been tested.[15] Here, we found that maximal respiration (stimulated by ADP+FCCP) was modestly suppressed by BCKAs in WT cardiac mitochondria (Figures 4C and 4D). Respiration of KO mitochondria, on the other hand, was significantly lower than in WT mitochondria in the absence of BCKAs, and BCKAs did not further suppress the respiration in KO cardiac mitochondria (Figures 4C and 4D). These results suggest that, unlike liver, inhibition of MPC by BCKAs plays a minor role in regulating pyruvate utilization in cardiac mitochondria.

An important difference in BCAA catabolism between the liver and the heart is that the liver lacks BCATm, which mediates reversible conversion between BCAAs and BCKAs.[38] We suspected that the BCATm reaction in cardiac mitochondria reduced the accumulation of BCKAs, thus alleviating the inhibitory effect on MPC. In support of the hypothesis, a recent study showed a strong inhibition of pyruvate oxidation by BCKAs in hearts deficient of BCATm.[39] Therefore, we compared the levels of BCAAs, the product, and glutamate, the donor of amino group in the BCATm reaction, in liver and heart mitochondria treated BCKAs. As expected, BCKAs caused no changes in BCAAs or glutamate levels in liver mitochondria due to the lack of BCATm (Figure 4E). In contrast, BCAA levels were significantly increased and glutamate levels were significantly decreased by BCKA treatment in heart mitochondria, suggesting a robust BCAT reaction converting BCKAs to BCAAs (Figure 4F). As the result, BCKA levels in liver KO mitochondria were significantly higher than cardiac KO mitochondria when exposed to the same concentration of BCKAs (Figure 4G). Moreover, we observed that the suppression of glucose production by BCKAs was significantly blunted by BCATm overexpression in hepatocytes (Figures 4H, 4I, and S4C). Finally, we measured BCKA levels in liver and heart and found that BCKA levels in the heart were marked lower than that in the liver for both WT and KO (Figure 4J).

DISCUSSION

The present study identifies a regulatory mechanism of MPC activity by BCKAs. When BCAA catabolism is impaired, accumulation of BCKAs inhibits mitochondrial MPC, resulting in the suppression of gluconeogenesis. This mechanism is prominent in liver due to the inherent lack of BCAT in hepatocytes, which renders inability to buffer the rise of BCKAs.

BCAA metabolism is closely related to glucose homeostasis, but the molecular mediator(s) in the regulatory circuit are elusive. Results of this study reveal a role of MPC in metabolic sensing and an additional mechanism of crosstalk between BCAA catabolism and glucose homeostasis. Impaired BCKA catabolism leads to substantially higher BCKA levels in the liver, which lacks BCATm compared with all other tissues in which BCATm is expressed.[16,28] Such a mechanism allows the liver to rapidly respond to changes in systemic

BCAA metabolism, and via regulating MPC activity, to achieve a new homeostasis of glucose metabolism. Corroborating our study, liver-specific MPC deficiency has been shown to reduce gluconeogenesis in obese mice. These findings suggest that liver BCKA levels could be a therapeutic target in glucose homeostasis.

Limitations of the study

While the study established a direct interaction between BCKA and MPC, the molecular basis for the inhibition of MPC activity was not defined. Future work that identifies the binding site of BCKAs, aided by the crystal structure of MPC when it becomes available, will be required to reveal the precise mechanism of inhibition. Furthermore, due to the lack of MPC overexpression animal model, the causal role of BCKA-mediated MPC inhibition in gluconeogenesis was not tested *in vivo*. Nevertheless, mice with liver-specific inhibition of BCKA catabolism showed better glucose tolerance when subjected to HFD feeding, thus supporting a key role of liver BCKA in glucose homeostasis.

STAR★METHODS

RESOURCE AVAILABILITY

Lead contact—Further information and requests for resources and reagents should be directed to and will be fulfilled by the lead contact, Rong Tian (rongtian@uw.edu).

Materials availability—All unique/stable reagents generated in this study are available from the lead contact with a completed materials transfer agreement.

Data and code availability—All data reported in this paper will be shared by the lead contact upon request. This paper does not report original code. Any additional information required to reanalyze the data reported in this paper is available from the lead contact upon request.

EXPERIMENTAL MODEL AND STUDY PARTICIPANT DETAILS

Animal studies—All animal experiments were performed with the approval by the Institutional Animal Care and Use Committee at the University of Washington (PPM1K KO and control WT mice) or the University of California at Los Angeles (Liver specific bckdha-knockout and control mice). All mice were housed at 22°C with a 12-h light, 12-h dark cycle with free access to water and standard chow or high fat diet (Research Diets, USA; D12492). PPM1K KO mice with C57BL/6 background were generated in our previous article.[5] Liver specific bckdha-knockout in mice was achieved by administration of AAV8 expressing Cre in a mouse line carrying bckdha$^{flox/flox}$ allele. For the Control group, AAV8-eGFP (Addgene: 105530-AAV8) was administered which was produced using pAAV-CMV-PI-EGFP-WPRE-bGH vector. For the bckdha liver knockout group, AAV8-Cre (Addgene: 107787-AAV8) was administered which was produced using pAAV-TBG-PI-Cre-rBG construct. The bckdha $^{flox/flox}$ mice were generated by inserting two *loxP* motifs flanking the exon 4 of mouse bckdha gene in C57B6J background. Genotype was confirmed by genomic DNA PCR. Ten weeks old bckdha $^{flox/flox}$ mice were injected intravenously with AAV8 viral solution at a dose of 1.5×10^{11} particles per mouse. Two weeks after AAV8

injection, high-fat diet treatment was commenced for 12 weeks before tissue collection. Male mice were used in this study except otherwise specified.

Primary hepatocytes and cell line—Mouse primary hepatocytes were obtained from male KO or wild-type mice by the two-step collagenase perfusion method.[42] Collagenase type II (Worthington Biochemical, USA; # CLS2)-digested liver was passed through a 70 mm cell strainer to obtain hepatocyte suspension. Then, mature hepatocytes were collected by centrifugation of the suspension. After isolation, hepatocytes were resuspended in DMEM supplemented with 5% FBS and 1% penicillin/streptomycin, and seeded on dishes coated by collagen type I (Cellmatrix type I-A, Nitta Gelatin Japan; #637–00653) at a density of 800,000cells/35mm dish. After over-night incubation under 5% CO2 at 95% humidity and 37°C, cells were used for experiments. HepG2 (Japanese Collection of Research Bioresources Cell Bank, Japan; JCRB1054) and HEK293T (RIKEN Bio Resource Research Center, Japan: RCB2202) were cultured in DMEM supplemented with 10% FBS and 1% penicillin/streptomycin under 5% CO2 at 95% humidity and 37°C.

METHOD DETAILS

Glucose, insulin, pyruvate, alanine and glycerol tolerance tests—Glucose tolerance test and insulin tolerance test were performed as follows, based on a previous study.[43] Mice were fasted for over-night (16–18 h), intraperitoneally injected with D-glucose solution (1–1.5g/kgBW, indicated in each figure) and blood samples were collected at the indicated time points. For insulin tolerance tests, mice were fasted for 5 h and intraperitoneally injected with insulin (Humulin R, Eli Lilly; 1–1.5 U/kg BW, indicated in each figure). For pyruvate, alanine or glycerol tolerance test, mice were fasted over-night (16–18 h) and intraperitoneally injected with pyruvate (0.75–1.5 g/kg BW, indicated in each figure), alanine (0.5 g/kg BW, indicated in each figure) or glycerol (2 g/kg BW, indicated in each figure) solution. Blood glucose levels were measured using a glucometer and serum insulin levels were determined by ELISA (Crystal Chem, USA; # 90080).

BT2 treatment—BT2 (3,6-dichlorobenzo[b]thiophene-2-carboxylic acid) treatment was performed as follows, based on a previous study.[15] Compound BT2 (Santa Cruz Biotechnology, USA; # sc-276559) was dissolved in 100% DMSO (100 mg/mL stock) and kept at 4°C until needed. Stock solution of BT2 was then diluted to a 10 mg/mL solution in 5% DMSO, 10% cremophor EL (Kolliphor EL, Sigma, USA; C5135), and 85% of 0.1 M Na-Bicarbonate, pH 9.0. For delivery, BT2 (40 mg/kg body weight/day) or vehicle (5% DMSO +10% cremophor EL + 85% of 0.L M Na-Bicarbonate) was administrated by daily oral gavage for 7 days.

Indirect calorimetry and body composition analysis—Indirect Calorimetry analysis was performed at the University of Washington, Nutrition Obesity Research Center (NORC) Energy Balance Core. 5 to 6-month-old WT and KO mice were first acclimated to metabolic cages connected to an indirect calorimetry system (Promethion, Sable Systems, USA). After a three-day acclimation period, O2 consumption, CO2 production, ambulatory activity (beam breaks), and food and water intake were recorded for three days. Data were collected

continuously at 5-min intervals, and respiratory exchange rate (RER) was calculated as a ratio of CO2 production to O2 consumption.

In vitro* glucose production assay—In vitro* glucose production assay was performed as follows, based on a previous study.[27] Isolated hepatocytes were placed in glucose production buffer containing 118 mM NaCl, 4.7 mM KCl, 1.2 mM MgSO4, 1.2 mM KH2PO4, 1.2 mM CaCl2, 20 mM NaHCO3, 25 mM HEPES pH 7.4, 0.025% BSA and 0.1mM 8-(4Chlorophenylthio) denosine 3′,5′-cyclic monophosphate sodium (pCPT-cAMP; Sigma, USA; #C3912). The buffer contains 0.4mM pyruvate +4.0mM lactate, 4mM glutamine, 4mM alanine or 0.5mM glycerol, unless otherwise indicated. BCKAs or 5μM UK5099 (sigma, USA; # PZ0160) was also added in the buffer when indicated. After incubated in the buffer for 5 h, conditioned medium was removed for glucose measurement and the hepatocytes were lysed with RIPA buffer. Glucose levels were measured by colorimetric assay (AUTOKIT Glucose, WAKO, Japan; # NC9927772) and the protein concentration was determined by Pierce BCA Protein Assay Kit (Thermo, USA; # 23227). For HepG2, 5μM dexamethasone (WAKO, Japan; #047–18863) was added to the medium over-night before the assay and 2mM pyruvate +20mM lactate + 5μM dexamethasone were added in the assay buffer, based on a previous study.[44]

Lentivirus production and infection—cDNAs encoding the full lengths of human MPC1, 2 or BCATm was cloned into a lenti vector pBOBI[40] by In-Fusion HD cloning kit (Takara Bio, Japan; #639648). The resulting lentiviral vectors (pBOBI-MPC1, 2 or BCATm) were transfected into HEK293T cells in the presence of lentivirus-packing plasmids (PMDL/REV/VSVG) using HilyMax (Dojindo, Japan, #H357) according to the manufacturer's instruction. After over-night incubation, cell culture medium was changed and the virus-containing medium was collected 22–26 h later. HepG2 is infected with lentiviral particles in the presence of 8 mg/mL polybrene and then centrifuged at 2500 g for 30 min.

Mitochondria isolation—Mouse liver and heart mitochondria were prepared as follows, based on a previous study.[45] Mouse liver was washed in ice-cold mitochondria isolation buffer (MIB; 70mM sucrose, 210mM mannitol, 5mM HEPES, 1mM EDTA and 0.5% fatty-acid BSA) and finely minced in 10 volumes of fresh MIB. The minced liver was homogenized on ice with Teflon glass homogenizer with three strokes at 1200 rpm using the overhear stirrer (Wheaton). For mice heart, digestion process by trypsin (0.1% trypsin, 10min, Sigma, USA) was added before homogenization and homogenate was prepared by four strokes at 1400 rpm using the overhear stirrer. Mitochondria was obtained from the homogenate by differential centrifugation. Briefly, the homogenate was centrifuged at 600g for 5 min at 4°C. The resulting pellet was resuspended in MIB and centrifuged at 8000g for 10 min at 4°C. After resuspending the final pellet in MIB buffer, concentration of mitochondria was determined by Pierce BCA protein assay kit (Thermo Scientific, USA; # 23227).

Pyruvate uptake assay—Mitochondrial pyruvate uptake was measured to assess MPC activity as previously reported[33,45] with modifications. Isolated liver mitochondria were

suspended in medium containing 70mM sucrose, 210mM mannitol, 5mM Tris-HCl, 0.5% fatty-acid free BSA and 1mM EDTA with pH7.4 in the concentration of 10 mg/mL mitochondrial protein. The protein concentration was determined by Pierce BCA Protein Assay Kit (ThermoScientific). An aliquot of the mitochondrial suspension (50μL or 0.5 mg of mitochondrial protein) was added to 150μL of uptake buffer containing 125mM KCl and 20mM Tris-HCl, pH 6.8. BCKAs were added to uptake buffer if described in each figure legends. The 200μL solution was incubated for 10 min at room temperature and transferred to a 0.4-mL centrifuge tube containing a layer of oil consisting of 1:37.5 n-dodecane:bromododecane (Sigma) during the incubation. After the 10 min incubation, [2–14C] pyruvate (15μM or 0.0225μCi) was spiked into the 200μL solution to start the assay. One minute after the spike, the mitochondria-associated radioactivity was separated from the medium by centrifugation at 12,535× g for 8 s. The portion of the tube containing the mitochondrial pellet was cut off with a razor blade, placed into a scintillation vial, and then counted for radioactivity.[46] Mitochondria pre-treated with 50mM UK5099 were used as a negative control and the radioactivity counts of UK5099-treated mitochondria were subtracted from the counts of non-pre-treated mitochondria. To measure the pyruvate uptake with 150μM pyruvate (Figures 3K and 3L), 15μM [2–14C] pyruvate was spiked with 135μM non-labelled pyruvate and the total amount of uptaken pyruvate was considered to be 10 times the amount of uptaken ^{14}C-pyruvate.

Measurement of mitochondria respiration—Mitochondrial respiration was calculated from oxygen consumption rates (OCRs) under specific conditions using an XF24 Extracellular Flux Analyzer (Seahorse Bioscience) based off the manufacturer's protocol.[47] Briefly, mitochondria isolated from liver were suspended in the mitochondrial assay solution (MAS; 70mM sucrose, 220mM mannitol, 10mM, KH2PO4, 5mM MgCl2, 2mM HEPES, 1mM EGTA, and 0.2% fatty acid free BSA; pH7.2 at room temperature). 10 μg mitochondria was loaded in the assay plate in a volume of 50μL MAS with pyruvate (10 mM)/malate (2 mM) or Glutamate (10mM)/Malate(2mM) as substrates. After centrifugation at 2000g for 20 min at 4°C, 450μL of MAS containing indicated substrates was added to each well, and the plate was incubated in a 37°C non-CO2incubator for 10 min. Then, ADP (4mM)/FCCP (4μM), UK5099 (50μM) and rotenone (4μM) were sequentially injected into each well.

Metabolite extraction—Metabolite extraction from hepatocytes, tissues or blood was performed as follows, based on a previous study.[48]

Hepatocyte: Isolated hepatocytes were placed in glucose production buffer containing 118 mM NaCl, 4.7 mM KCl, 1.2 mM MgSO4, 1.2 mM KH2PO4, 1.2 mM CaCl2, 20 mM NaHCO3, 25 mM HEPES pH 7.4, 0.025% BSA, 0.1mM 8-(4Chlorophenylthio) denosine 3′,5′-cyclic monophosphate sodium (pCPT-cAMP; Sigma, USA; #C3912), 0.4mM pyruvate and 4.0mM lactate. BCKAs or 5μM UK5099 (sigma, USA; # PZ0160) was also added in the buffer when indicated. For carbon-tracing experiments in Figure 3F, U^{13}C-pyruvate (Cambridge Isotope Laboratories, USA; #CLM-2440) was used instead of non-labelled pyruvate. After incubated in the buffer for 2 h, hepatocytes were washed with 0.9% NaCl and harvested in 80% methanol: 20% H2O. Internal standard (methyl succinate, Sigma

Aldrich) was added before homogenization. After centrifugation, aqueous extracts were dried in a Speed-Vac at 30°C.

Tissue samples: 20–25 mg of freeze-clamped liver or gastrocnemius muscle were homogenized in 2:1 chloroform: methanol with internal standard (methyl succinate, Sigma Aldrich). After adding 1:1 chloroform: water solution, the samples were vortexed and placed on ice for 30 min. Aqueous extracts obtained by centrifugation (2000 rpm for 20 min) and filter (0.22μm) were dried in a Speed-Vac at 30°C.

Serum: 10μL of serum was placed on ice for 60 min after being mixed with 100uL methanol. Aqueous extracts obtained by centrifugation were dried in a Speed-Vac at 30°C.

Mass spectrometry—Gas chromatography-mass spectrometry (GCMS) was performed as follows, based on a previous study.[48] For derivatization, dried aqueous extracts were incubated with 20 mg/mL methoxyaminehydrochloride in pyridine (Sigma Aldrich) for 90 min at 37°C followed by MTBSTFA (Sigma Aldrich) for 30 min at 70°C. FAME standard (Sigma Aldrich) was spiked into samples before loading samples into GC autosampler vials. All samples were analyzed using an Agilent 7890 GC instrument equipped with a 5977-mass selective detector (MSD), employing an HP-5MS UI GC column. GCMS conditions were used according to the Fiehn library instructions from Agilent.[49,50] Retention time of individual metabolites were annotated according to known standards. Peak intensities were normalized to total ion count (TIC) and protein concentration and depicted as fold change from control. KIV, KMV levels were measured with Xevo TQ-S Q-TOF and an Aquity UPLC HILIC Column (Waters Corporation, USA).[51]

To calculate the BCKA concentration in hepatocytes, cell volume was estimated from protein concentration of cell lysates. Based on previous literature,[52] we assumed that protein amount is 20%w/v of cell volume in hepatocytes for both KO and WT.

Immunoblot analysis—Liver homogenates, isolated mouse liver mitochondria or isolated hepatocyte lysates were prepared as follows, based on a previous study.[53] Samples were lysed in RIPA buffer containing 50 mM Tris (pH 7.4), 150 mM NaCl, 1% Triton X-100, 0.1% SDS, protease inhibitor cocktail (Roche) and phosphatase inhibitor cocktail (Sigma). After proteins were transferred to a PVDF membrane, immunoblots were probed with the indicated antibodies. ImageJ[41] was used for densitomeric quantification.

DARTs (drug affinity responsive target stability) assay—DARTs assay was performed as follows, based on previous studies.[35,36] Liver from wild-type C57BL/6 mice were lysed using M-PER ((Thermo Scientific, 78501) supplemented with protease inhibitors (Roche, #11836153001). TNC buffer (50 mM Tris-HCl pH 8.0, 50 mM NaCl, 10 mM CaCl2) was added to the lysate and protein concentration was then determined using the BCA Protein Assay kit (Thermo, USA; # 23227). The lysates were incubated with either vehicle (H2O) or 1mM BCKAs for 60 min on ice followed by additional 15 min at room temperature. Digestion was performed using Pronase (Roche, 10165921001) at 25°C for 30 min (MPC1,2) or 5 min (GAPDH) and stopped by adding NuPAGE LDS loading buffer (Invitrogen, NP0008) and immediately heating at 70°C for 10 min. Samples were subjected

to SDS–PAGE on 4–12% Bis-Tris gradient gel (Invitrogen, NP0323BOX). After the proteins were transferred to PVDF, immunoblots were probed with MPC1,2 or GAPDH.

Quantitative real-time PCR (qRT-PCR) analysis—Total RNA was purified using Trizol reagent (Invitrogen) according to the manufacturer's protocol. First-strand cDNA was synthesized from total RNA using the Transcriptor First Strand cDNA Synthesis Kit (Roche). qRT-PCR was carried out using 7900HT Real-Time PCR System (Applied Biosystems) and iQ SYBR Green Supermix (Bio Rad) following the manufacturers' directions. The results were standardized for comparison by measuring the level of 36B4 mRNA in each sample.

Lactate and β-Hydroxybutyrate measurement—Serum lactate and β-Hydroxybutyrate levels were determined by L-Lactate Assay Kit (Cayman chemical) and EnzyChrom Ketone Body Assay Kit (BioAssay Systems), respectively.

QUANTIFICATION AND STATISTICAL ANALYSIS

Results are expressed as mean ± SEM. Graphpad prism 9 was used to calculate the statistics. Student's t test was used for comparisons between two groups. One-way ANOVA with post hoc Tukey-Kramer test or two-way ANOVA with post hoc Sidak test was used for comparisons among multiple groups. For the comparison of metabolites, multiple t test with two-stage step-up method of Benjamini, Krieger and Yekutieli (False discovery rate <0.01) was used.

Supplementary Material

Refer to Web version on PubMed Central for supplementary material.

ACKNOWLEDGMENTS

The authors are grateful to Drs. Gary Lopaschuk and Qutuba Karwi for the helpful discussion on cardiac-specific BCATm KO mice and to the members of the Tian lab for their support of the study. We are also grateful to Varun Kamat and Boriboun Chantharangkoul for technical support. pAAV.CMV.-PI.EGFP.WPRE.bGH and AAV.TBG.PI.Cre.rBG were gifts from James M. Wilson. The graphical abstract was created with BioRender. This work was supported in part by National Institutes of Health grants HL-118989 (to R.T.) and HL-R01 HL140116 (to Y.W. and C.G.); by the Department of Defense/CDMRP PR191680 (to C.G. and Y.W.); by P30 DK017047 (to Diabetes Research Center Cell Function Analysis Core); by fellowships from the Japan Heart Foundation (to K.N. and A.Y.), the Uehara Memorial Foundation (grant no. 202040002 to A.Y.), and the American Heart Association (grant no. 827259 to A.Y.); and by JSPS grants-in-Aid for scientific research (21K20867 and 23K07966 to K.N.).

INCLUSION AND DIVERSITY

We support inclusive, diverse, and equitable conduct of research.

REFERENCES

1. Lynch CJ, and Adams SH (2014). Branched-chain amino acids in metabolic signalling and insulin resistance. Nat. Rev. Endocrinol. 10, 723–736. 10.1038/nrendo.2014.171. [PubMed: 25287287]
2. Chuang DT, Chuang JL, and Wynn RM (2006). Lessons from genetic disorders of branched-chain amino acid metabolism. J. Nutr. 136, 243S–249S. 10.1093/jn/136.1.243s. [PubMed: 16365091]

3. Pettit FH, Yeaman SJ, and Reed LJ (1978). Purification and characterization of branched chain α-keto acid dehydrogenase complex of bovine kidney. Proc. Natl. Acad. Sci. USA 75, 4881–4885. 10.1073/pnas.75.10.4881. [PubMed: 283398]
4. Popov KM, Zhao Y, Shimomura Y, Kuntz MJ, and Harris RA (1992). Branched-chain alpha-ketoacid dehydrogenase kinase. Molecular cloning, expression, and sequence similarity with histidine protein kinases. J. Biol. Chem. 267, 13127–13130. [PubMed: 1377677]
5. Lu G, Sun H, She P, Youn J-Y, Warburton S, Ping P, Vondriska TM, Cai H, Lynch CJ, and Wang Y (2009). Protein phosphatase 2Cm is a critical regulator of branched-chain amino acid catabolism in mice and cultured cells. J. Clin. Invest. 119, 1678–1687. 10.1172/jci38151. [PubMed: 19411760]
6. Newgard C, An J, Bain J, and Muehlbauer M (2009). A branched-chain amino acid-related metabolic signature that differentiates obese and lean humans and contributes to insulin resistance. Cell Metab. 9, 311–326. [PubMed: 19356713]
7. Newgard CB (2012). Interplay between lipids and branched-chain amino acids in development of insulin resistance. Cell Metab. 15, 606–614. 10.1016/j.cmet.2012.01.024. [PubMed: 22560213]
8. Shah SH, Crosslin DR, Haynes CS, Nelson S, Turer CB, Stevens RD, Muehlbauer MJ, Wenner BR, Bain JR, Laferrère B, et al. (2012). Branched-chain amino acid levels are associated with improvement in insulin resistance with weight loss. Diabetologia 55, 321–330. 10.1007/s00125-011-2356-5. [PubMed: 22065088]
9. White PJ, Lapworth AL, An J, Wang L, McGarrah RW, Stevens RD, Ilkayeva O, George T, Muehlbauer MJ, Bain JR, et al. (2016). Branched-chain amino acid restriction in Zucker-fatty rats improves muscle insulin sensitivity by enhancing efficiency of fatty acid oxidation and acyl-glycine export. Mol. Metab. 5, 538–551. 10.1016/j.molmet.2016.04.006. [PubMed: 27408778]
10. Palmer ND, Stevens RD, Antinozzi PA, Anderson A, Bergman RN, Wagenknecht LE, Newgard CB, and Bowden DW (2015). Metabolomic profile associated with insulin resistance and conversion to diabetes in the insulin resistance atherosclerosis study. J. Clin. Endocrinol. Metab. 100, E463–E468. 10.1210/jc.2014-2357. [PubMed: 25423564]
11. White PJ, McGarrah RW, Grimsrud PA, Tso S-C, Yang W-H, Haldeman JM, Grenier-Larouche T, An J, Lapworth AL, Astapova I, et al. (2018). The BCKDH kinase and phosphatase integrate BCAA and lipid metabolism via regulation of ATP-citrate lyase. Cell Metab. 27, 1281–1293.e7. 10.1016/j.cmet.2018.04.015. [PubMed: 29779826]
12. Lotta LA, Scott RA, Sharp SJ, Burgess S, Luan J, Tillin T, Schmidt AF, Imamura F, Stewart ID, Perry JRB, et al. (2016). Genetic predisposition to an impaired metabolism of the branched-chain amino acids and risk of type 2 diabetes: a mendelian randomisation analysis. PLoS Med. 13, e1002179. 10.1371/journal.pmed.1002179. [PubMed: 27898682]
13. Wang Q, Holmes MV, Davey Smith G, and Ala-Korpela M (2017). Genetic support for a causal role of insulin resistance on circulating branched-chain amino acids and inflammation. Diabetes Care 40, 1779–1786. 10.2337/dc17-1642. [PubMed: 29046328]
14. Wang TJ, Larson MG, Vasan RS, Cheng S, Rhee EP, McCabe E, Lewis GD, Fox CS, Jacques PF, Fernandez C, et al. (2011). Metabolite profiles and the risk of developing diabetes. Nat. Med. 17, 448–453. [PubMed: 21423183]
15. Li T, Zhang Z, Kolwicz SC, Abell L, Roe ND, Kim M, Zhou B, Cao Y, Ritterhoff J, Gu H, et al. (2017). Defective branched-chain amino acid catabolism disrupts glucose metabolism and sensitizes the heart to ischemia-reperfusion injury. Cell Metab. 25, 374–385. 10.1016/j.cmet.2016.11.005. [PubMed: 28178567]
16. Sun H, Olson KC, Gao C, Prosdocimo DA, Zhou M, Wang Z, Jeyaraj D, Youn J-Y, Ren S, Liu Y, et al. (2016). Catabolic defect of branched-chain amino acids promotes heart failure. Circulation 133, 2038–2049. 10.1161/circulationaha.115.020226. [PubMed: 27059949]
17. Wang J, Liu Y, Lian K, Shentu X, Fang J, Shao J, Chen M, Wang Y, Zhou M, and Sun H (2019). BCAA catabolic defect alters glucose metabolism in lean mice. Front. Physiol. 10, 1140. 10.3389/fphys.2019.01140. [PubMed: 31551816]
18. Green CR, Wallace M, Divakaruni AS, Phillips SA, Murphy AN, Ciaraldi TP, and Metallo CM (2016). Branched-chain amino acid catabolism fuels adipocyte differentiation and lipogenesis. Nat. Chem. Biol. 12, 15–21. 10.1038/nchembio.1961. [PubMed: 26571352]

19. Fontana L, Cummings NE, Arriola Apelo SI, Neuman JC, Kasza I, Schmidt BA, Cava E, Spelta F, Tosti V, Syed FA, et al. (2016). Decreased consumption of branched-chain amino acids improves metabolic Health. Cell Rep. 16, 520–530. 10.1016/j.celrep.2016.05.092. [PubMed: 27346343]
20. Zhou M, Shao J, Wu C-Y, Shu L, Dong W, Liu Y, Chen M, Wynn RM, Wang J, Wang J, et al. (2019). Targeting BCAA catabolism to treat obesity-associated insulin resistance. Diabetes 68, 1730–1746. 10.2337/db18-0927. [PubMed: 31167878]
21. Harper AE, Miller RH, and Block KP (1984). Branched-chain amino acid metabolism. Annu. Rev. Nutr. 4, 409–454. 10.1146/annurev.nu.04.070184.002205. [PubMed: 6380539]
22. Neinast MD, Jang C, Hui S, Murashige DS, Chu Q, Morscher RJ, Li X, Zhan L, White E, Anthony TG, et al. (2019). Quantitative analysis of the whole-body metabolic fate of branched-chain amino acids. Cell Metab. 29, 417–429.e4. 10.1016/j.cmet.2018.10.013. [PubMed: 30449684]
23. Jang C, Oh SF, Wada S, Rowe GC, Liu L, Chan MC, Rhee J, Hoshino A, Kim B, Ibrahim A, et al. (2016). A branched-chain amino acid metabolite drives vascular fatty acid transport and causes insulin resistance. Nat. Med. 22, 421–426. 10.1038/nm.4057. [PubMed: 26950361]
24. Magnusson I, Rothman DL, Katz LD, Shulman RG, and Shulman GI (1992). Increased rate of gluconeogenesis in type II diabetes mellitus. A 13C nuclear magnetic resonance study. J. Clin. Invest. 90, 1323–1327. 10.1172/jci115997. [PubMed: 1401068]
25. Rines AK, Sharabi K, Tavares CDJ, and Puigserver P (2016). Targeting hepatic glucose metabolism in the treatment of type 2 diabetes. Nat. Rev. Drug Discov. 15, 786–804. 10.1038/nrd.2016.151. [PubMed: 27516169]
26. Hatting M, Tavares CDJ, Sharabi K, Rines AK, and Puigserver P (2018). Insulin regulation of gluconeogenesis. Ann. N. Y. Acad. Sci. 1411, 21–35. 10.1111/nyas.13435. [PubMed: 28868790]
27. Axelsson AS, Tubbs E, Mecham B, Chacko S, Nenonen HA, Tang Y, Fahey JW, Derry JMJ, Wollheim CB, Wierup N, et al. (2017). Sulforaphane reduces hepatic glucose production and improves glucose control in patients with type 2 diabetes. Sci. Transl. Med. 9, eaah4477. 10.1126/scitranslmed.aah4477. [PubMed: 28615356]
28. Olson KC, Chen G, and Lynch CJ (2013). Quantification of branched-chain keto acids in tissue by ultra fast liquid chromatography–mass spectrometry. Anal. Biochem. 439, 116–122. 10.1016/j.ab.2013.05.002. [PubMed: 23684523]
29. Miller RA, Shi Y, Lu W, Pirman DA, Jatkar A, Blatnik M, Wu H, Cárdenas C, Wan M, Foskett JK, et al. (2018). Targeting hepatic glutaminase activity to ameliorate hyperglycemia. Nat. Med. 24, 518–524. 10.1038/nm.4514. [PubMed: 29578539]
30. Gray LR, Sultana MR, Rauckhorst AJ, Oonthonpan L, Tompkins SC, Sharma A, Fu X, Miao R, Pewa AD, Brown KS, et al. (2015). Hepatic mitochondrial pyruvate carrier 1 is required for efficient regulation of gluconeogenesis and whole-body glucose homeostasis. Cell Metab. 22, 669–681. 10.1016/j.cmet.2015.07.027. [PubMed: 26344103]
31. McCommis KS, Chen Z, Fu X, McDonald WG, Colca JR, Kletzien RF, Burgess SC, and Finck BN (2015). Loss of mitochondrial pyruvate carrier 2 in the liver leads to defects in gluconeogenesis and compensation via pyruvate-alanine cycling. Cell Metab. 22, 682–694. 10.1016/j.cmet.2015.07.028. [PubMed: 26344101]
32. Cunningham CN, and Rutter J (2020). 20,000 picometers under the OMM: diving into the vastness of mitochondrial metabolite transport. EMBO Rep. 21, e50071. 10.15252/embr.202050071. [PubMed: 32329174]
33. Du J, Cleghorn WM, Contreras L, Lindsay K, Rountree AM, Chertov AO, Turner SJ, Sahaboglu A, Linton J, Sadilek M, et al. (2013). Inhibition of mitochondrial pyruvate transport by zaprinast causes massive accumulation of aspartate at the expense of glutamate in the retina. J. Biol. Chem. 288, 36129–36140. 10.1074/jbc.m113.507285. [PubMed: 24187136]
34. Yang J, Copeland RA, and Lai Z (2009). Defining balanced conditions for inhibitor screening assays that target bisubstrate enzymes. J. Biomol. Screen 14, 111–120. 10.1177/1087057108328763. [PubMed: 19196704]
35. Lomenick B, Hao R, Jonai N, Chin RM, Aghajan M, Warburton S, Wang J, Wu RP, Gomez F, Loo JA, et al. (2009). Target identification using drug affinity responsive target stability (DARTS). Proc. Natl. Acad. Sci. USA 106, 21984–21989. 10.1073/pnas.0910040106. [PubMed: 19995983]

36. Chin RM, Fu X, Pai MY, Vergnes L, Hwang H, Deng G, Diep S, Lomenick B, Meli VS, Monsalve GC, et al. (2014). The metabolite α-ketoglutarate extends lifespan by inhibiting ATP synthase and TOR. Nature 510, 397–401. 10.1038/nature13264. [PubMed: 24828042]
37. Diether M, and Sauer U (2017). Towards detecting regulatory protein–metabolite interactions. Curr. Opin. Microbiol. 39, 16–23. 10.1016/j.mib.2017.07.006. [PubMed: 28810194]
38. Sivanand S, and Vander Heiden MG (2020). Emerging roles for branched-chain amino acid metabolism in cancer. Cancer Cell 37, 147–156. 10.1016/j.ccell.2019.12.011. [PubMed: 32049045]
39. Uddin GM, Karwi QG, Pherwani S, Gopal K, Wagg CS, Biswas D, Atnasious M, Wu Y, Wu G, Zhang L, et al. (2021). Deletion of BCATm increases insulin-stimulated glucose oxidation in the heart. Metabolis 124, 154871. 10.1016/j.metabol.2021.154871.
40. Miyoshi H, Blömer U, Takahashi M, Gage FH, and Verma IM (1998). Development of a self-inactivating lentivirus vector. J. Virol. 72, 8150–8157. 10.1128/jvi.72.10.8150-8157.1998. [PubMed: 9733856]
41. Schneider CA, Rasband WS, and Eliceiri KW (2012). NIH Image to ImageJ: 25 years of image analysis. Nat. Methods 9, 671–675. 10.1038/nmeth.2089. [PubMed: 22930834]
42. Horie T, Nishino T, Baba O, Kuwabara Y, Nakao T, Nishiga M, Usami S, Izuhara M, Sowa N, Yahagi N, et al. (2013). MicroRNA-33 regulates sterol regulatory element-binding protein 1 expression in mice. Nat. Commun. 4, 2883. 10.1038/ncomms3883. [PubMed: 24300912]
43. Nishi K, Sato Y, Ohno M, Hiraoka Y, Saijo S, Sakamoto J, Chen P-M, Morita Y, Matsuda S, Iwasaki K, et al. (2016). Nardilysin is required for maintaining pancreatic β-cell function. Diabetes 65, 3015–3027. 10.2337/db16-0178. [PubMed: 27385158]
44. Sen S, Sanyal S, Srivastava DK, Dasgupta D, Roy S, and Das C (2017). Transcription factor 19 interacts with histone 3 lysine 4 trimethylation and controls gluconeogenesis via the nucleosome-remodeling-deacetylase complex. J. Biol. Chem. 292, 20362–20378. 10.1074/jbc.m117.786863. [PubMed: 29042441]
45. Gray LR, Rauckhorst AJ, and Taylor EB (2016). A method for multiplexed measurement of mitochondrial pyruvate carrier activity. J. Biol. Chem. 291, 7409–7417. 10.1074/jbc.m115.711663. [PubMed: 26823462]
46. Sweet IR, Cook DL, Lernmark Å, Greenbaum CJ, Wallen AR, Marcum ES, Stekhova SA, and Krohn KA (2004). Systematic screening of potential β-cell imaging agents. Biochem. Biophys. Res. Commun. 314, 976–983. 10.1016/j.bbrc.2003.12.182. [PubMed: 14751228]
47. Rogers GW, Brand MD, Petrosyan S, Ashok D, Elorza AA, Ferrick DA, and Murphy AN (2011). High throughput microplate respiratory measurements using minimal quantities of isolated mitochondria. PLoS One 6, e21746. 10.1371/journal.pone.0021746. [PubMed: 21799747]
48. Ritterhoff J, Young S, Villet O, Shao D, Neto FC, Bettcher LF, Hsu Y-WA, Kolwicz SC, Raftery D, and Tian R (2020). Metabolic remodeling promotes cardiac hypertrophy by directing glucose to aspartate biosynthesis. Circ. Res. 126, 182–196. 10.1161/circresaha.119.315483. [PubMed: 31709908]
49. You R, Dai J, Zhang P, Barding GA, and Raftery D (2018). Dynamic metabolic response to adriamycin-induced senescence in breast cancer cells. Metabolites 8, 95. 10.3390/metabo8040095. [PubMed: 30558288]
50. Kind T, Wohlgemuth G, Lee DY, Lu Y, Palazoglu M, Shahbaz S, and Fiehn O (2009). FiehnLib: mass spectral and retention index libraries for metabolomics based on quadrupole and time-of-flight gas chromatography/mass spectrometry. Anal. Chem. 81, 10038–10048. 10.1021/ac9019522. [PubMed: 19928838]
51. Li R, Liu P, Liu P, Tian Y, Hua Y, Gao Y, He H, Chen J, Zhang Z, and Huang Y (2016). A novel liquid chromatography tandem mass spectrometry method for simultaneous determination of branched-chain amino acids and branched-chain α-keto acids in human plasma. Amino Acids 48, 1523–1532. 10.1007/s00726-016-2212-5. [PubMed: 26984321]
52. Brown GC (1991). Total cell protein concentration as an evolutionary constraint on the metabolic control distribution in cells. J. Theor. Biol. 153, 195–203. 10.1016/s0022-5193(05)80422-9. [PubMed: 1787736]

53. Shao D, Kolwicz SC, Wang P, Roe ND, Villet O, Nishi K, Hsu Y-WA, Flint GV, Caudal A, Wang W, et al. (2020). Increasing fatty acid oxidation prevents high fat diet induced cardiomyopathy through regulating parkin mediated mitophagy. Circulation 142, 983–997. 10.1161/circulationaha.119.043319. [PubMed: 32597196]

Highlights

- Gluconeogenesis is impaired in mice with decreased BCAA catabolism due to *Ppm1k* deficiency
- BCKAs selectively inhibit pyruvate-supported glucose production in hepatocytes
- BCKAs inhibit mitochondrial pyruvate carrier (MPC) in hepatocytes
- BCATm in non-hepatocytes protects against BCKA accumulation, alleviates the inhibition of MPC

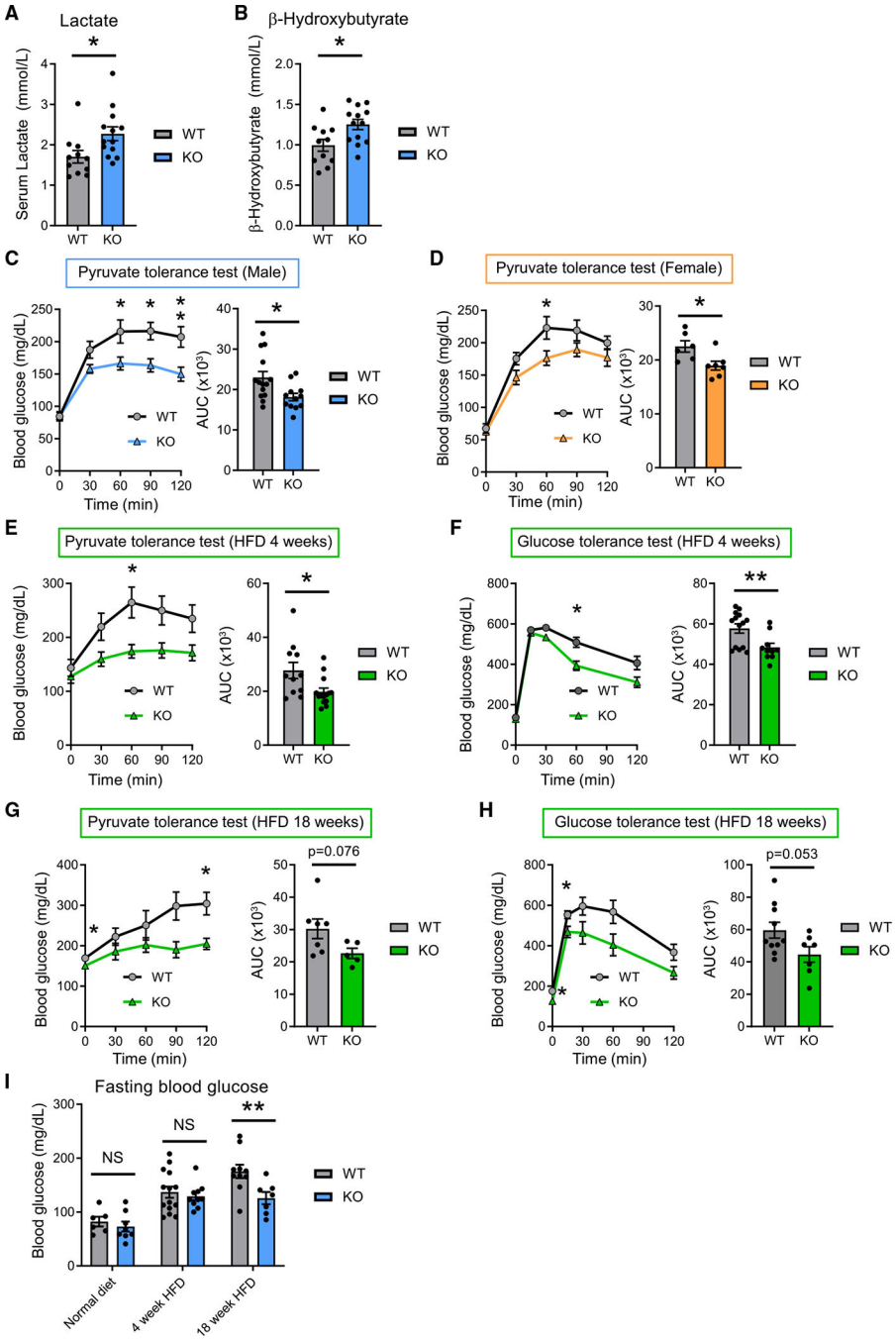

Figure 1. PPM1K KO mice showed reduced gluconeogenesis and protected from HFD-induced glucose intolerance

(A and B) Serum lactate (A) and β-hydroxybutyrate (B) levels of 6-month-old *Ppm1k*$^{-/-}$ (KO) and wild-type (WT) mice after overnight fasting (n = 11–14).

(C and D) Pyruvate tolerance test in 6-month-old male (n = 12–14; C) or female (n = 6–7; D) KO and WT mice after intraperitoneal (i.p.) injection of 1.5 g pyruvate/kg body weight.

(E and F) Pyruvate tolerance test (1 g pyruvate/kg i.p., n = 11–14; E) or glucose tolerance test (1 g glucose/kg i.p., n = 10–14; F) in KO and WT mice fed with HFD for 4 weeks.

(G and H) Pyruvate tolerance test (1 g pyruvate/kg i.p., n = 5–7; G) or glucose tolerance test (1 g glucose/kg i.p., n = 7–10; H) in KO and WT mice fed with HFD for 18 weeks.
(I) Fasting blood glucose levels of KO and WT mice fed with normal chow diet or HFD (n = 6–14).
Data are presented as mean ± SEM. *p < 0.05, **p < 0.01. p values were determined using unpaired Student's t test (A–H), one-way ANOVA with post hoc Tukey-Kramer test (I), or two-way ANOVA with post hoc Sidak test (C–H).

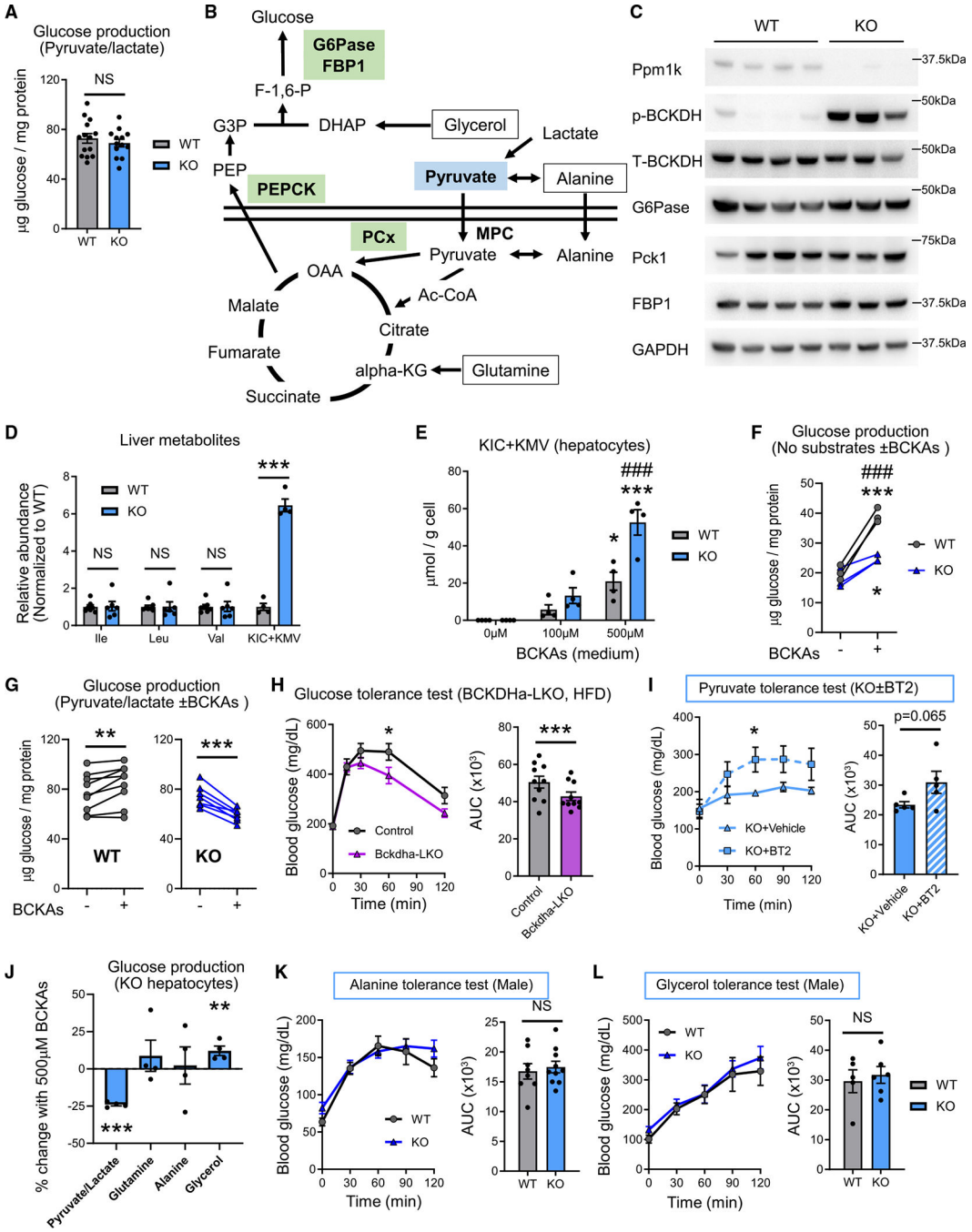

Figure 2. Pyruvate-supported glucose production is specifically suppressed in BCKA-treated hepatocytes and PPM1K KO mice

(A) Glucose production in primary hepatocytes treated with glucose production assay buffer (with 0.4 mM pyruvate and 4 mM lactate) for 5 h (n = 13–14).

(B) Metabolites and enzymes involved in gluconeogenic pathway.

(C) Immunoblot of liver lysate of 6-month-old *Ppm1k*$^{-/-}$ (KO) and WT mice.

(D) BCAA and BCKA levels in liver from 6-month-old fasted WT or KO mice, which was determined by GC-MS (BCAAs) or liquid chromatography-MS (LC-MS; BCKAs) (n = 4–6).

(E) α-ketoisocaproate (KIC) and α-keto-β-methylvalerate (KMV) levels in primary hepatocytes incubated with glucose production assay buffer containing 0.4 mM pyruvate, 4 mM lactate, and increasing concentrations of BCKAs for 5 h (*$p < 0.05$ vs. WT with 0 μM BCKAs, ***$p < 0.001$ vs. KO with 0 μM BCKAs, ###$p < 0.001$ vs. WT with 500 μM BCKAs, n = 4).

(F) Glucose production of primary hepatocytes treated with glucose production assay buffer without pyruvate/lactate for 5 h. Measurements were made with or without BCKAs (500 μM) (*$p < 0.05$ vs. KO without BCKAs, ***$p < 0.001$ vs. WT without BCKAs, ###$p < 0.001$ vs. WT with BCKAs, n = 3).

(G) Glucose production of primary hepatocytes treated with glucose production assay buffer containing 0.4 mM pyruvate and 4 mM lactate for 5 h. Measurements were made with or without BCKAs (500 μM) (n = 9 each).

(H) Glucose tolerance test (1.5 g glucose/kg i.p.) in HFD-fed hepatocyte-specific *Bckdha*-deficient (BCKDHa-LKO) and AAV-EGFP-injected control mice (n = 10).

(I) Pyruvate tolerance test (1.5 g pyruvate/kg i.p.) in 6-month-old KO mice treated with either BT2 (3,6-dichlorobenzo[b]thiophene-2-carboxylic acid, 40 mg/kg body weight/day, oral gavage) or vehicle (5% DMSO, 10% cremophor EL, and 85% 0.L M Na-bicarbonate) for 7 days (n = 5 each).

(J) Percentage of change of glucose production by 500 μM BCKAs in KO hepatocytes treated with glucose production buffer containing 0.4 mM pyruvate + 4 mM lactate, 4 mM glutamine, 4 mM alanine, or 0.5 mM glycerol (n = 4 each).

(K and L) Alanine (0.5 g/kg, i.p., n = 8–10; K) or glycerol (2 g/kg i.p., n = 8–10; L) tolerance test in male KO and WT mice.

Data are presented as mean ± SEM. NS, not significant, *$p < 0.05$, **$p < 0.01$, ***$p < 0.001$, unless otherwise indicated. p values were determined using unpaired (A, H, I, K, and L) or paired (G and J) Student's t test or two-way ANOVA with post hoc Sidak test (D–F, H, I, K, and L).

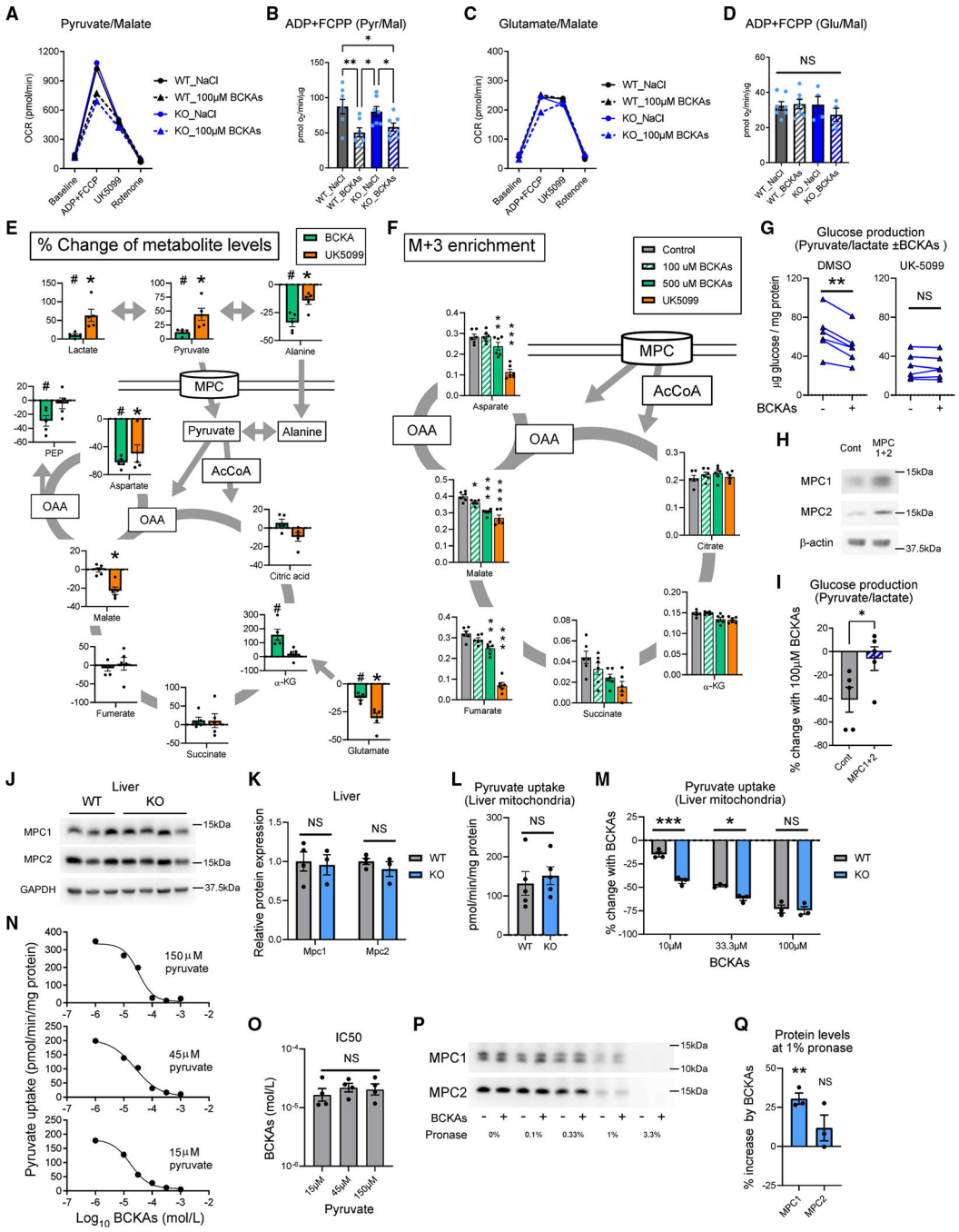

Figure 3. BCKAs directly inhibit MPC activity in non-competitive manner

(A and B) Representative results of oxygen consumption rate (OCR) in liver mitochondria supplied with 10 mM pyruvate/2 mM malate and treated with 100 μM BCKA-Na or NaCl (A) and the quantification of maximum respiration (B; n = 7).

(C and D) Representative results of OCR in liver mitochondria supplied with10 mM glutamate/2 mM malate and treated with 100 μM BCKA-Na or NaCl (C) and the quantification of maximum respiration (D; n = 4–7).

(E) Metabolite levels in primary hepatocytes treated with glucose production assay buffer containing 0.4 mM pyruvate and 4 mM lactate for 2 h. Data are shown as percentage of changes induced by 500 μM BCKAs or 5 μM UK5099 compared with vehicle (#, significant change by BCKAs; *, significant change by UK5099, n = 5).
(F) M+3 enrichment of TCA cycle metabolites in primary hepatocytes from KO mice treated with glucose production assay buffer containing 0.4 mM $U^{13}C$-pyruvate and 4 mM lactate plus increasing concentrations of BCKAs or 5 μM UK5099 for 2 h (n = 6).
(G) UK5099 cancels the inhibitory effect of BCKAs on glucose production in KO hepatocytes treated with glucose production buffer containing pyruvate+lactate. DMSO was used as vehicle control (n = 6).
(H) Immunoblot of control and MPC1+2-overexpressed HepG2 cells.
(I) Percentage of change of glucose production by 100 μM BCKAs in MPC1+2-overexpressed and control HepG2 (n = 5 each).
(J) Immunoblot of liver lysate from 6-month-old WT and KO mice.
(K) Densitomeric quantification of MPC1 and MPC2. GAPDH was used as internal control (n = 3–4).
(L) ^{14}C-pyruvate uptake of liver mitochondria isolated from WT and KO mice (n = 5).
(M) Percentage of change of pyruvate uptake by increasing concentrations of BCKAs in WT or KO liver mitochondria (n = 3).
(N) Representative dose-response curve for the inhibition of pyruvate uptake by BCKAs (10^{-6} to 10^{-3} mol/L) measured at 15, 45, or 150 μM pyruvate.
(O) Average IC50 of BCKAs at pyruvate concentration of 15, 45, or 150 μM (n = 4 independent experiments).
(P) Representative immunoblots of liver lysate digested by protease mixture (pronase) at increasing doses for 30 min at 25°C with or without 1 mM BCKAs.
(Q) The effect of BCKAs on the protein amount at 1% pronase relative to the amount at 0% pronase. Data are quantified by densitometry and expressed as percentage change by BCKAs over no BCKAs (n = 3).
Data are presented as mean ± SEM. NS, not significant, *$p < 0.05$, **$p < 0.01$ ***$p < 0.001$. p values were determined using unpaired (I and L) or paired (G and Q) Student's t test, one-way ANOVA with post hoc Tukey-Kramer test (B, D, and O), two-way ANOVA with post hoc Sidak test (F, K, and M), or multiple t test with two-stage step-up method of Benjamini, Krieger, and Yekutieli (E; false discovery rate < 0.01).

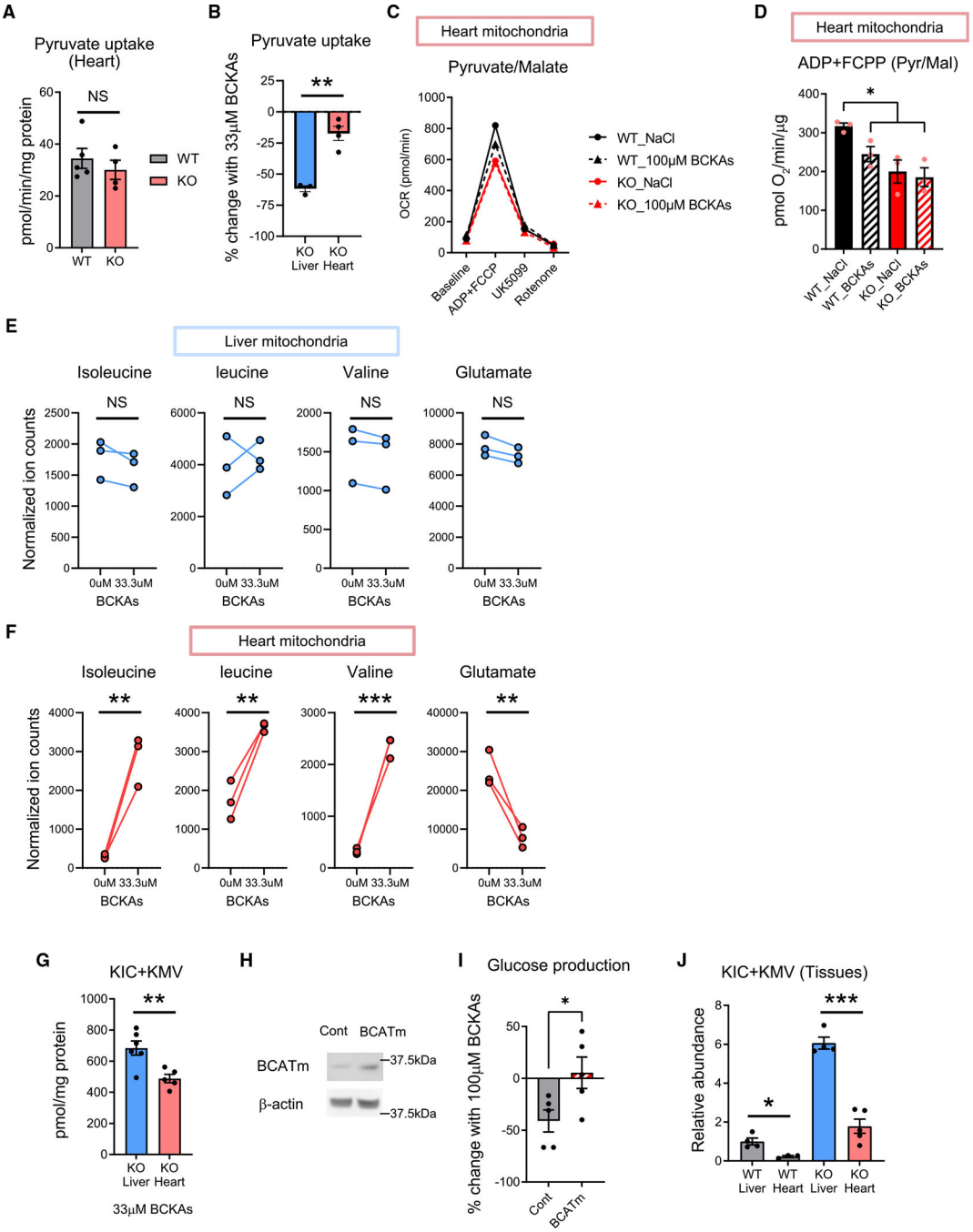

Figure 4. BCKAs' effects on MPC activity are attenuated in non-liver mitochondria by BCAT expression

(A) ^{14}C-pyruvate uptake of cardiac mitochondria isolated from WT and KO mice (n = 4–5).

(B) Percentage of change of pyruvate uptake caused by 33.3 μM BCKAs in KO liver or heart mitochondria (n = 3–4).

(C and D) Representative results of OCR in heart mitochondria supplied with 10 mM pyruvate/1 mM malate and treated with 100μM BCKA-Na or NaCl (C) and the quantification of maximum respiration (D; n = 3).

(E and F) Isoleucine, leucine, valine, and glutamate levels in cardiac (E) or liver (F) mitochondria isolated from KO mice, and treated with 0 or 33.3mM BCKAs (n = 3).
(G) KIC+KMV levels in KO liver and heart mitochondria treated with 33 μM BCKAs (n = 5).
(H) Immunoblot of control and BCATm-overexpressed HepG2 cells.
(I) Percentage of change of glucose production from pyruvate and lactate by 100 μM BCKAs in BCATm-overexpressed and control HepG2 (n = 5).
(J) KIC+KMV levels of liver and heart from WT and KO (n = 3–5).
Data are presented as mean ± SEM. NS, not significant, *p < 0.05, **p < 0.01 ***p < 0.001. p values were determined using unpaired (A, B, G, and I) Student's t test, one-way ANOVA with post hoc Tukey-Kramer test (D), and multiple t test with two-stage step-up method of Benjamini, Krieger, and Yekutieli (E, F, and J; false discovery rate < 0.01).

KEY RESOURCES TABLE

REAGENT or RESOURCE	SOURCE	IDENTIFIER
Antibodies		
Rabbit polyclonal to PPM1K	Abcam	# ab135286; RRID: AB_2889377
Rabbit polyclonal to BCKDHA (phospho S293)	Abcam	# ab200577; RRID: AB_2687944
Rabbit polyclonal to BCKDHA	Abcam	# ab126173; RRID: AB_11131209
Rabbit polyclonal to G6Pase	Novus Biologicals	# NBP1-80533; RRID: AB_11044224
Rabbit polyclonal to PCK1	Abcam	# ab70358; RRID: AB_1925305
Rabbit monoclonal to FBP1	Cell Signaling Technology	# 72736; RRID: AB_2799827
Rabbit monoclonal to GAPDH	Cell Signaling Technology	#2118; RRID: AB_561053
Rabbit monoclonal to MPC1	Cell Signaling Technology	# 14462; RRID: AB_2773729
Rabbit monoclonal to MPC2	Cell Signaling Technology	# 46141; RRID: AB_2799295
Rabbit monoclonal to VDAC	Cell Signaling Technology	# 4661; RRID: AB_10557420
Rabbit polyclonal to BCATm	Proteintech	# 16417-1-AP; RRID: AB_10792411
Mouse monoclonal to beta actin	Santa Cruz	# sc-47778; RRID: AB_626632
Chemicals, peptides, and recombinant proteins		
$^{13}C_3$-pyruvate	Cambridge Isotope Laboratories	# CLM-2440-
Hily max	Dojindo	#H357
Collagen type I (Cellmatrix type I-A)	Nitta Gelatin	# 637-00653
Pyruvic Acid, Sodium Salt, [2-14C]	PerkinElmer	# NEC256050UC
3,6-dichloro-benzo[b]thiophene-2-Carboxylic Acid	Santa Cruz Biotechnology	# sc-276559
Kolliphor EL	Sigma	#C5135
8-(4Chlorophenylthio) denosine 3′,5′-cyclic monophosphate sodium	Sigma	#C3912
UK-5099	Sigma	# PZ0160
TRIzol	Thermo Fisher Scientific	#15596018
Dexamethasone	WAKO	#047-18863
Collagenase, Type 2	Worthington Biochemical	# CLS2
Critical commercial assays		
EnzyChrom™ Ketone body Assay Kit	BioAssay Systems	# EKBD-100
L-Lactate Assay Kit	Cayman Chemical	# 700510
Ultra Sensitive Mouse Insulin ELISA Kit	Crystal Chem	# 90080
Verso cDNA Synthesis Kit	Thermo Fisher Scientific	# AB1453B
BCA Protein Assay	Thermo Fisher Scientific	# 23227
In-Fusion HD cloning kit	Takara Bio	# 639648
AUTOKIT GLUCOSE C2	WAKO	# NC9927772
Experimental models: Cell lines		
HepG2	Japanese Collection of Research Bioresources Cell Bank	# JCRB1054

REAGENT or RESOURCE	SOURCE	IDENTIFIER
HEK293T	RIKEN BRC (BioResource Research Center)	RCB2202
Experimental models: Organisms/strains		
Mouse: *Ppm1k*$^{-/-}$	Lu et al.[5]	N/A
Mouse: *Bckdha*$^{loxP/loxP}$	This article	N/A
Mouse: C57BL/6J	The Jaxon Laboratory	Catalog # 000664; RRID: IMSR_JAX:000664
Oligonucleotides		
Primers for qPCR, see Table S2	This article	N/A
Primers for subcloning of human BCATm, MPC1 and 2, see Table S2	This article	N/A
Recombinant DNA		
pAAV-CMV-PI-EGFP-WPRE-bGH	Addgene	#105530
AAV.TBG.PI.Cre.rBG	Addgene	#107787
pBOBI	Miyoshi et al.[40]	N/A
pBOBI-MPC1	This article	N/A
pBOBI-MPC2	This article	N/A
pBOBI-BCATm	This article	N/A
Software and algorithms		
Graphpad prism	GraphPad software	https://www.graphpad.com/
ImageJ	Schneider et al.[41]	https://imagej.nih.gov/ij/
MassLynx 4.1	Waters Corporation	https://www.waters.com/waters/en_US/MassLynx-MS-Software/nav.htm?locale=en_US&cid=513662
BioRender	BioRender	https://www.biorender.com/